Strongly nonresonant four-wave mixing in semiconductors

W.-R. Hannes ●,[1] A. Trautmann,[1] M. Stein ●,[2] F. Schäfer ●,[2] M. Koch ●,[2] and T. Meier ●[1]

[1]*Department of Physics and CeOPP, University of Paderborn, Warburger Strasse 100, D-33098 Paderborn, Germany*
[2]*Department of Physics and Materials Science Center, Philipps-Universität Marburg, Renthof 5, D-35032 Marburg, Germany*

When semiconductors are optically excited above or slightly below the band gap, the linear and nonlinear responses originate predominantly from the interband polarization. Here, we demonstrate that intraband excitations, i.e., rapidly oscillating currents that originate from the electric-field-induced acceleration of electrons and holes, contribute strongly to transient four-wave mixing when it is performed with center frequencies near half the band gap frequency. Within a two-band model we show that the presence of several pathways arising from different combinations of inter- and intraband excitations and their interference give rise to characteristic signatures in time- and spectrally resolved signals. Our approach is based on the semiconductor Bloch equations and includes the dynamics of off-resonant electron-hole excitations on a microscopic level. The predicted significant broadening and structure appearing in the four-wave-mixing spectra are in good qualitative agreement with experimental results.

I. INTRODUCTION

Coherent four-wave mixing (FWM) is a well-established method to study light-matter interaction and the dynamics of material excitations on ultrafast timescales [1–20]. A common variation is the so-called self-diffraction geometry in which two laser pulses with wave vectors $\mathbf{k}_1$ and $\mathbf{k}_2$ that are delayed with respect to each other by a time delay τ are focused onto a sample under a small angle. While the first pulse generates a macroscopic polarization $P^{(1)}(t)$ in the sample, the second pulse acts in two ways. In the first step it interacts with the polarization induced by the first pulse, creating a population grating of the electronic states. In the second step it interacts with this grating and creates a polarization $P^{(3)}(t, \tau)$ which is at least of third order, depends on the time delay τ and real time t, and acts as the source of the FWM signal that is emitted in the direction of $2\mathbf{k}_2 - \mathbf{k}_1$ [19–21]. FWM spectroscopy allows for the determination of dephasing times even in inhomogeneously broadened systems (see, e.g., [2,9,10,12,19–22]). Furthermore, the coupling between electronic states can be revealed [6,8,23,24], and many-body effects, e.g., excitonic effects [4,5,12,19,20,25], and many-body correlations such as biexcitonic contributions [11,17,19,20,22,26–37] and excitation-induced dephasing [38–42] were successfully analyzed using FWM spectroscopy and its extensions, e.g., two-dimensional Fourier-transform spectroscopy [23,43–46].

In nearly all cases reported so far the electronic transitions have been excited resonantly or with a small detuning. However, there have been a few reports on FWM experiments carried out with photon energies far below the energy of the fundamental optical transition in the respective material. The only experiments on semiconductors which are known to us have been carried out by Gur-Arie and Bar-Ad, who investigated GaAs and InP using mid-band-gap pulses [47]. They found a spectral shift and a broadening of the FWM

signal which they attributed to an impulsive excitation of symmetric lattice vibrations. Reif *et al.* [48] studied BaF_2 and attributed the observed diffracted orders to Kerr grating, i.e., a spatial modulation of the samples' refractive index originating from the Kerr effect. They showed that the lifetime of the grating is limited by the temporal width of the laser pulses. Further experiments were performed on glasses (fused silica and BK7) and BaF_2 [49] as well as the nonlinear crystal $LiNbO_3$ [50]. For the latter, also a spectral broadening of the FWM signal was observed. Yet none of these papers contained any microscopic theory which describes the dynamics of the off-resonantly excited electronic transitions which are responsible for the FWM emission.

It is well known that for experiments which involve nonresonant excitation the assumption that the nonlinear response originates solely from the interband polarization is invalid. For example, recently, several experiments where solid-state systems are excited with highly intense terahertz (THz) pulses showed the generation of high harmonics up to optical frequencies [51–56] which can be understood properly only when both inter- and intraband excitations are taken into account [57–63]. The same is true for, e.g., two- and multiphoton absorption and emission [64–70] as well as the excitation of photocurrents with two-color fields [71–76].

In this paper, we study a setting that is somehow in between resonant interband and THz optics. We analyze FWM for the case of strongly nonresonant excitation performed with pulses that have a center frequency close to half of the band gap frequency. Unlike previous studies [48–50], where an instantaneous Kerr nonlinearity was taken as the source of the FWM emission, our approach includes the dynamics of off-resonant electron-hole excitations on a microscopic level. Model calculations for a slab with a homogeneous density of two-level systems using the Maxwell-Bloch equation show that the nonlinearity of the two-level systems, which originates

from Pauli blocking (also known as phase-space filling), gives rise to a density grating off which an electromagnetic field is scattered into the FWM direction. For the more realistic two-band model we demonstrate that in this case intraband excitations contribute strongly to FWM signals. In semiconductors the interference of several pathways which correspond to different combinations of inter- and intraband excitations results in characteristic modifications of the time- and spectrally resolved signals. In particular, significant broadening and an additional structure are predicted to appear in the FWM spectra. Our numerical results are compared with experiments, and we obtain good qualitative agreement of several features. Although we do observe two or more peaks in some of the measured FWM spectra, we, unlike the results of Ref. [47], do not find a clear correlation with phonon frequencies of the investigated materials.

This paper is organized as follows: In Sec. II we describe our theoretical approach and present and discuss our numerical results. After starting with a simple two-level system we show the modifications that appear within a two-band model when both inter- and intraband excitations are taken into account in the framework of the semiconductor Bloch equations (SBEs). In addition, supporting results which include propagation via the Maxwell-Bloch equations for a two-dimensional model are provided in the Appendix. The experimental results are presented and discussed in Sec. III. Our main results are briefly summarized in Sec. IV.

II. THEORETICAL APPROACH AND SIMULATION RESULTS

In this section we describe our theoretical models and present and discuss our numerical results. We first consider a two-level system in Sec. II A and show that already for this simplest model nonresonant interband excitations lead to a finite FWM signal. In the time domain the width of this coherent nonlinear signal is smaller than that of the incident pulse envelopes, and correspondingly, the FWM spectra are broadened in comparison to the spectra of the exciting pulses. Additional simulations including propagation for a two-dimensional model system, which are presented in the Appendix, shine additional light on the generation of the FWM emission and confirm our findings.

Clearly, a two-level system is too simple to describe optical excitations of bulk semiconductors as well as extended nanostructures like quantum wells and wires where the electronic states appear in bands and are given by extended Bloch functions. Therefore we present and analyze in Sec. II B a two-band model which includes both inter- and intraband excitations. For the two-band model it is demonstrated that for strongly nonresonant excitation besides the interband polarization also intraband currents contribute significantly to FWM. Due to the interference of several terms the FWM signals differ significantly from the two-level results. In particular, the destructive interference between two contributions may lead to two peaks in both the time-resolved and the spectrally resolved FWMs. For simplicity, we restrict our analysis to the third-order limit and thus compute the FWM signal in the perturbative regime, and in addition many-body and propagation effects are neglected in this initial model

study. Although it is known that excitonic effects and many-body correlations strongly dominate FWM for resonant excitation, in the regime considered here the detuning is the largest relevant energy scale, and we therefore do not expect strong modifications arising from many-body contributions. This assumption is verified by the qualitative agreement of our theoretical results with experiment (see Sec. III).

A. Two-level model

Many nonlinear optical processes, e.g., bleaching and the optical Stark effect as measured in pump-probe experiments, FWM including photon echoes in inhomogeneously broadened systems, Rabi oscillations, etc., have been successfully described using a simple two-level model. The well-known Bloch equations for a two-level system read [19–21,77]

$$\frac{\partial}{\partial t} p = -i\omega_{cv} p + \frac{i}{\hbar} \mathbf{d} \cdot \mathbf{E}(1 - 2n) - \frac{p}{T_2}, \quad (1)$$

$$\frac{\partial}{\partial t} n = \frac{i}{\hbar} \mathbf{d} \cdot \mathbf{E}(p^* - p) - \frac{n}{T_1}, \quad (2)$$

where p is the interband coherence between the two levels and n is the occupation of the upper level. ω_{cv} is the transition frequency, $\mathbf{d}$ is the dipole matrix element between the two states, and $\mathbf{E}(t)$ is the electric field driving the optical excitation. The decay of the interband coherence is modeled phenomenologically by the dephasing time T_2, and relaxation is modeled by the time T_1 which describes the decay into the lower level whose occupation is given by $(1 - n)$. The optical response of the two-level system is governed by the interband polarization $\mathbf{P}(t) = \mathbf{d}(p + p^*)$.

The optical excitation is modeled by considering two laser pulses, and the total electric field is given by $\mathbf{E}(t) = \mathbf{E}_1(t) + \mathbf{E}_2(t)$, with $\mathbf{E}_\nu = \hat{\mathbf{e}}_\nu E_\nu(t)$ and $E_\nu(t) = \hat{E}_\nu(t) \cos(\mathbf{k}_\nu \cdot \mathbf{r} - \omega_L t)$ for $\nu = 1, 2$. The pulses are colinearly polarized $\hat{\mathbf{e}}_1 = \hat{\mathbf{e}}_2 = \mathbf{d}/|\mathbf{d}| \equiv \hat{\mathbf{e}}$, are degenerate, and have a Gaussian envelope with the same duration $\hat{E}_1(t) = \hat{E}_2(t) \propto e^{-(t/\bar{t})^2}$. As is well known, for resonant or near-resonant excitation, i.e., $\omega_L \approx \omega_{cv}$, an interband polarization $\mathbf{P}^{(3)}_{FWM}$ is generated in third order in the light-matter interaction whose second time derivative is the source of the FWM signal emitted in the direction of $2\mathbf{k}_2 - \mathbf{k}_1$. In a perturbative analysis of this signal one starts with an interband coherence $p^{(1)}$ induced by $\mathbf{E}_1$ which by the interaction with $\mathbf{E}_2$ is conjugated and transferred into a second-order density grating $n^{(2)}$. By another interaction with $\mathbf{E}_2$ this grating leads to a third-order interband coherence $p^{(3)}$ which is responsible for the FWM emission.

This scenario including the perturbative analysis also holds for a strongly nonresonant excitation when the detuning $\Delta = \omega_{cv} - \omega_L$ exceeds all other relevant frequency scales, i.e., the spectral width of the laser pulses and the homogeneous linewidth. However, in the fully off-resonant case one enters the following adiabatic regime [19,77] in which the dynamics of the coherent material excitations follows the envelope of the exciting pulse (often, such excitations are referred to as *virtual*). In this regime $p^{(1)}$ induced by the first pulse is proportional to $\Delta^{-1}\hat{E}_1(t)e^{-i\omega_L t}$ [where we have neglected the contribution proportional to $(\omega_{cv} + \omega_L)^{-1}\hat{E}_1(t)e^{i\omega_L t}$, which is even weaker for a not too small ω_L]. Since $p^{(1)}$ exists only as long as $\mathbf{E}_1$ is present, a FWM signal can be generated only
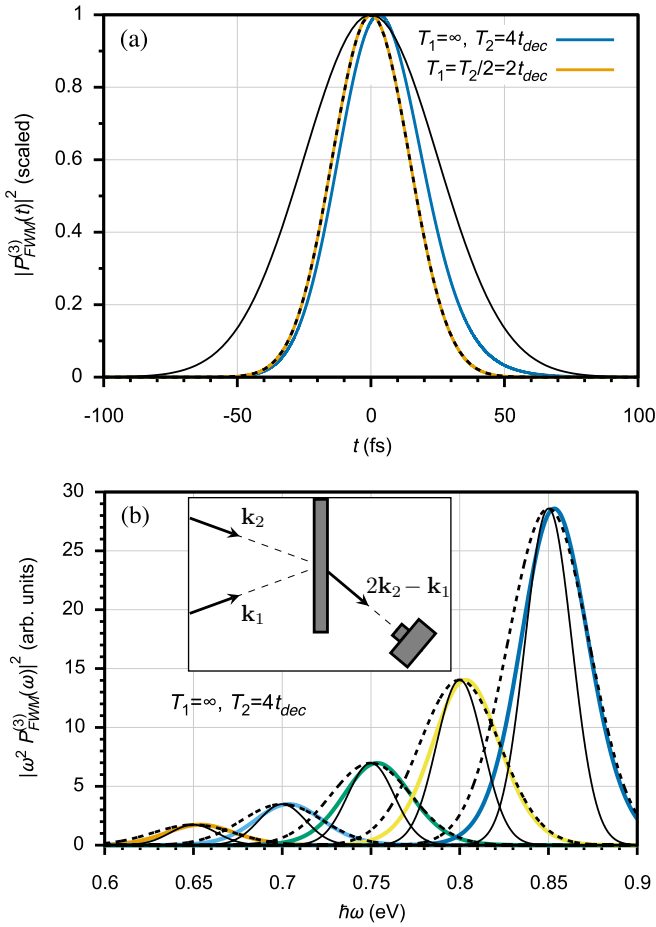
FIG. 1. (a) FWM signal in the time domain for $\hbar\omega_L = 0.8$ eV (corresponding to $\lambda_L = 1550$ nm). The black solid and dashed lines show the square of the pulse envelope, i.e., $[\hat{E}(t)]^2$, and its third power $[\hat{E}(t)]^6$, respectively. (b) FWM signal in the frequency domain for different $\hbar\omega_L$ (thick colored lines). The black solid and dashed lines show the squared Fourier transforms of $E(t)$ and $[E(t)]^3$, i.e., $|E(\omega)|^2$ and $|E(\omega)|^6$, respectively. In both (a) and (b) we use $\bar{t} = 50$ fs and $\hbar\omega_{cv} = 1.5$ eV, which is close to the band gap of GaAs.

when the two pulses overlap in time. We therefore limit the present analysis to the case of zero time delay between the pulses, i.e., $\hat{E}_1(t) = \hat{E}_2(t) \equiv \hat{E}(t)$. Also in third order $p^{(3)}(t)$ is generated off resonantly, and it thus vanishes directly after the excitation. Its magnitude scales as Δ^{-3}, and since three excitations are involved, its dynamics should be more rapid than the envelope of the incident pulses and rather behave as $[\hat{E}(t)]^\alpha$ with an α close to 3.

These theoretical expectations are fully confirmed by numerical solutions of the two-level Bloch equations, Eqs. (1) and (2). As shown in Fig. 1(a) in the coherent limit, i.e., $T_2 = 2T_1$, the FWM intensity $\mathbf{I}_{FWM}(t) \propto |\mathbf{P}^{(3)}_{FWM}(t)|^2$ is nearly identical to $[\hat{E}(t)]^6$. However, this limit is very unrealistic for extended semiconductor systems where the dephasing is typically much more rapid than relaxation. For $T_2 \ll T_1$ the temporal dynamics of $|\mathbf{P}^{(3)}_{FWM}(t)|^2$ is a bit delayed and slightly slower than $|\mathbf{E}(\omega)|^6$, but this retardation is significant only if T_2 is comparable to or smaller than the pulse length $\bar{t}$. Correspondingly, even away from the coherent limit, the spectrally resolved FWM intensity $\mathbf{I}^{(3)}_{FWM}(\omega) \propto |\omega^2 \mathbf{P}^{(3)}_{FWM}(\omega)|^2$ appears

to be significantly broader than the width of the intensity of the incident pulses $|\mathbf{E}(\omega)|^2$ [see Fig. 1(b)]. Our numerical simulations confirm that the overall scaling of the FWM intensity is close to $\omega_L^4 \Delta^{-6}$, as expected for a nonresonant excitation.

B. Two-band model

Although a two-level system is sufficient to demonstrate the existence of FWM in the strongly nonresonant regime, this simple model does not adequately describe the excitation of extended semiconductors in this regime. The main shortcoming of the two-level model is that it includes only interband excitations but completely misses intraband excitations. Whereas intraband excitations, i.e., the electric-field-induced acceleration of electrons within a band, are typically negligible for resonant excitation with frequencies near or above the band gap, they contribute significantly to the optical response when semiconductors are excited with low-frequency fields, e.g., to high-harmonic generation induced by THz fields. Other examples where inter- and intraband excitations contribute and interfere are, e.g., multiphoton absorption and the excitation of photocurrents with two-color fields.

In the following we demonstrate that intraband excitations need to be considered when analyzing FWM in the strongly nonresonant regime and that in addition to the interband polarization the intraband current has to be included as a source for the FWM signal. Our analysis is based on the Bloch equations for two bands which include both interband ($\propto \mathbf{d} \cdot \mathbf{E}$) and intraband ($\propto \mathbf{E} \cdot \nabla_\mathbf{k}$) excitations [58,70,76],

$$\frac{\partial}{\partial t} p_\mathbf{k} = -i\omega_\mathbf{k} p_\mathbf{k} + \frac{i}{\hbar}\mathbf{d} \cdot \mathbf{E}(1 - 2n_\mathbf{k})$$
$$+ \frac{e}{\hbar}\mathbf{E} \cdot \nabla_\mathbf{k} p_\mathbf{k} - \frac{p_\mathbf{k}}{T_2}, \tag{3}$$

$$\frac{\partial}{\partial t} n_\mathbf{k} = \frac{i}{\hbar}\mathbf{d} \cdot \mathbf{E}(p_\mathbf{k}^* - p_\mathbf{k}) + \frac{e}{\hbar}\mathbf{E} \cdot \nabla_\mathbf{k} n_\mathbf{k} - \frac{n_\mathbf{k}}{T_1}. \tag{4}$$

The interband polarization for the two-band system is given by $\mathbf{P}(t) = \mathbf{d} \int d\mathbf{k} \ (p_\mathbf{k} + p_\mathbf{k}^*)$. Unlike the two-level system, however, in this case the time derivative of the total current $\mathbf{J}(t) = \mathbf{J}_p(t) + \mathbf{J}_n(t)$, with

$$\mathbf{J}_p(t) = \frac{\partial}{\partial t}\mathbf{P}(t), \tag{5}$$

$$\mathbf{J}_n(t) = -e \int d\mathbf{k} \ n_\mathbf{k} \nabla_\mathbf{k}\omega_\mathbf{k}, \tag{6}$$

needs to be considered as the source for the nonlinear optical signals. It should be noted that for a transition frequency $\omega_\mathbf{k}$ which is symmetric as a function of $\mathbf{k}$, its derivative is asymmetric, and thus $\mathbf{J}_n(t)$ is finite only if the occupation $n_\mathbf{k}$ has contributions which are asymmetric in $\mathbf{k}$ space.

Considering a two-band system that is in its ground state before the optical excitation, i.e., $p_\mathbf{k} = n_\mathbf{k} = 0$, the linear optical response is fully described by $p_\mathbf{k}^{(1)}$, which originates from an interband excitation. The dynamics of $p_\mathbf{k}^{(1)}$ is proportional to $\Delta_\mathbf{k}^{-1}\hat{E}_1(t)e^{-i\omega_L t}$ and thus, apart from a weak $\mathbf{k}$ dependence of the detuning $\Delta_\mathbf{k} = \omega_\mathbf{k} - \omega_L$, identical to that of $p^{(1)}$ for the two-level system. So in the linear optical regime the two-band model just corresponds to a summation over

many two-level systems representing the interband transitions at different points in **k** space.

In the nonlinear regime, however, additional excitations appear in the two-band model which do not exist in a two-level system. At second order in the light-matter interaction, in addition to $n_{\mathbf{k}}^{(2)}$ it is also possible to generate $p_{\mathbf{k}}^{(2)}$ via an intraband excitation [70,76,78]. It should be noted that within the present model with a symmetric interband transition frequency $\omega_{\mathbf{k}}$ and a symmetric (actually, **k**-independent) dipole matrix element **d**, $p_{\mathbf{k}}^{(2)}$ is asymmetric as a function of **k** and thus after summing over **k** does not lead to a macroscopic second-order polarization. At third order, $p_{\mathbf{k}}^{(3)}$ ($n_{\mathbf{k}}^{(3)}$) can be generated by an interband (intraband) excitation from $n_{\mathbf{k}}^{(2)}$ as well as by an intraband (interband) excitation from $p_{\mathbf{k}}^{(2)}$. Although for the two-level system only a single pathway, corresponding to three consecutive interband excitations, leads to FWM, for the two-band model four contributions exist, and in addition to $p_{\mathbf{k}}^{(3)}$ also $n_{\mathbf{k}}^{(3)}$ is generated, demonstrating that intraband currents contribute to FWM.

For our numerical solutions of Eqs. (3) and (4) we consider a finite T_2 (of 150 fs in Figs. 2 and 3) and an infinite T_1 since in semiconductors the dephasing is typically much more rapid than the relaxation. The following discussion holds for a broad range of parameter values (T_2, $\bar{t}$, λ_L); however, below we also discuss features that are sensitive to the excitation and system parameters.

Figure 2(a) shows that the FWM signal originating from the polarization current $|\mathbf{J}_p(t)|^2$ has basically a Gaussian shape with a peak near $t \approx 0$ and thus is quite similar to the signal obtained for the two-level system. The population current $|\mathbf{J}_n(t)|^2$, however, shows a more complex behavior and has two peaks as a function of time. Furthermore, the maximum of $|\mathbf{J}_n(t)|^2$ exceeds that of $|\mathbf{J}_p(t)|^2$, clearly demonstrating the relevance of intraband excitations. The total signal is determined by $|\mathbf{J}_p(t) + \mathbf{J}_n(t)|^2$, and thus it contains an interference contribution given by $[\mathbf{J}_p(t)\mathbf{J}_n^*(t) + \mathbf{J}_p^*(t)\mathbf{J}_n(t)]$. As shown in Fig. 2(a) the interference between the polarization and the current contributions is positive for times smaller than about 20 fs, then becomes negative, and for longer times is again positive. The total signal has a minimum at about 30 fs which is close to the maximal negative interference between $\mathbf{J}_p(t)$ and $\mathbf{J}_n(t)$ where these two terms almost cancel each other.

The change from the initially constructive to destructive interference between $\mathbf{J}_p(t)$ and $\mathbf{J}_n(t)$ has its origin basically in a phase change of $\mathbf{J}_n(t)$ as a function of time [see Fig. 2(b)]. $\mathbf{J}_n(t)$ is generated from two second-order sources, i.e., $p_{\mathbf{k}}^{(2)}$ and $n_{\mathbf{k}}^{(2)}$. Whereas the contribution originating from $p_{\mathbf{k}}^{(2)}$ follows the dynamics of the incident pulses, the contribution originating from $n_{\mathbf{k}}^{(2)}$ has a slightly delayed maximum. It should be noted that this temporal shift originates from our choice of a long (in fact, infinite) T_1 time, and it is absent in the coherent limit, which, however, is very unrealistic for semiconductors. Furthermore, the two contributions to $\mathbf{J}_n(t)$ have a phase difference of π and thus interfere destructively.

The opposite sign of the two terms can also be verified by calculating $\mathbf{J}_n(t)$ analytically. The term of $n_{\mathbf{k}}^{(3)}$ originating from $p_{\mathbf{k}}^{(2)}$ is proportional to $[i(\omega_{\mathbf{k}} - 2\omega_L) + (1/T_2)]^{-1}$. Thus when $2\hbar\omega_L$ exceeds the band gap, resonant two-photon
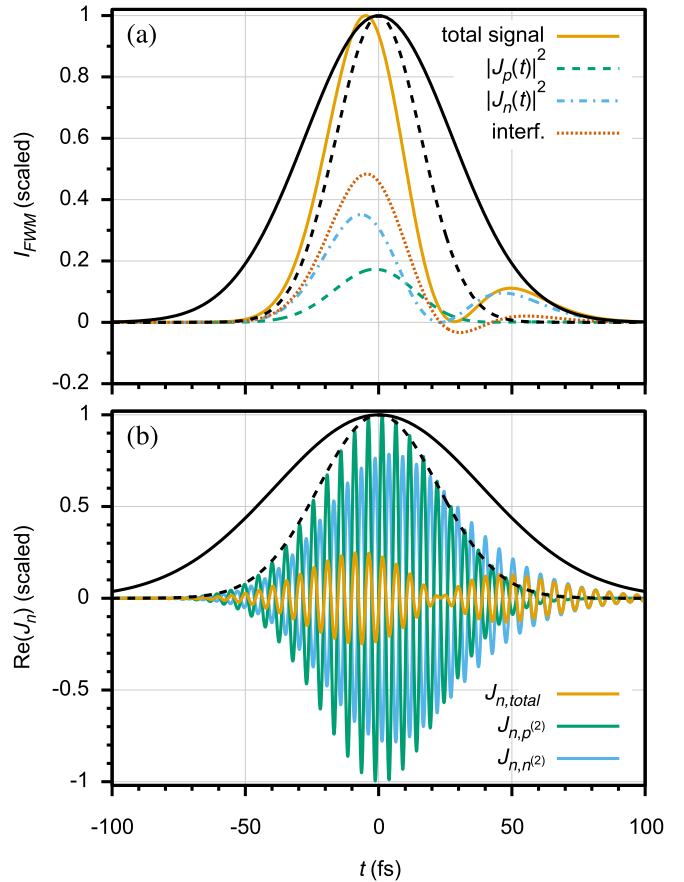
FIG. 2. (a) FWM intensity in the time domain $|\mathbf{J}_p(t) + \mathbf{J}_n(t)|^2$ along with individual contributions. (b) Real part of the density contribution $J_n \equiv \hat{\mathbf{e}} \cdot \mathbf{J}_n$ [compare Eq. (6)] to the FWM directed third-order current density. The total J_n is a sum of two contributions, $J_{n,p^{(2)}}$ and $J_{n,n^{(2)}}$, which are also shown. In (b) the black solid and dashed lines correspond to $\hat{E}(t)$ and $[\hat{E}(t)]^3$, respectively. In (a) these envelopes are squared and shown by the same line types. The parameters are $\lambda_L = 1550$ nm ($\hbar\omega_L \simeq 0.8$ eV), $\bar{t} = 55$ fs, $T_1 = \infty$, $T_2 = 150$ fs, $\hbar\omega_{\mathbf{k}=0} = 1.58$ eV, $m_e^* = 0.1m_0$, $m_h^* = 0.5m_0$, $|\mathbf{d}| = 3e$ Å; that is, the material parameters closely correspond to GaAs.

excitations are included in $p_{\mathbf{k}}^{(2)}$. However, the FWM is dominated by off-resonant excitations, and therefore the sign of this contribution to $\mathbf{J}_n(t)$ depends on whether most interband transition frequencies $\omega_{\mathbf{k}}$ are larger or smaller than $2\omega_L$. If $2\omega_L$ is only slightly above the band gap, as in the situation considered in Fig. 2, most $\omega_{\mathbf{k}}$ are larger than $2\omega_L$. In this case the signs of $J_{n,p^{(2)}}$ and $J_{n,n^{(2)}}$, i.e., the contributions originating from the two sources of $n_{\mathbf{k}}^{(3)}$, are opposite, which leads to the strong destructive interference of the two terms shown in Fig. 2(b). Even for higher-frequency excitation, $\omega_{\mathbf{k}}$ is, on average, larger than $2\omega_L$; however, the phase shift is not exactly π, and the minimum in the double-peak structure of $|\mathbf{J}_n(t)|^2$ and I_{FWM} does not reach zero as in Fig. 2(a). Due to their shifted temporal dynamics, first, the source term originating from $p_{\mathbf{k}}^{(2)}$ is dominant, whereas later, the one from $n_{\mathbf{k}}^{(2)}$ is larger, which leads to the two peaks in the envelope of $\mathbf{J}_n(t)$ and the phase shift near its minimum at around 20 fs. In principle, the FWM signal originating from the polarization current $|\mathbf{J}_p(t)|^2$ shows the same behavior; however, in this case, the delayed peak is
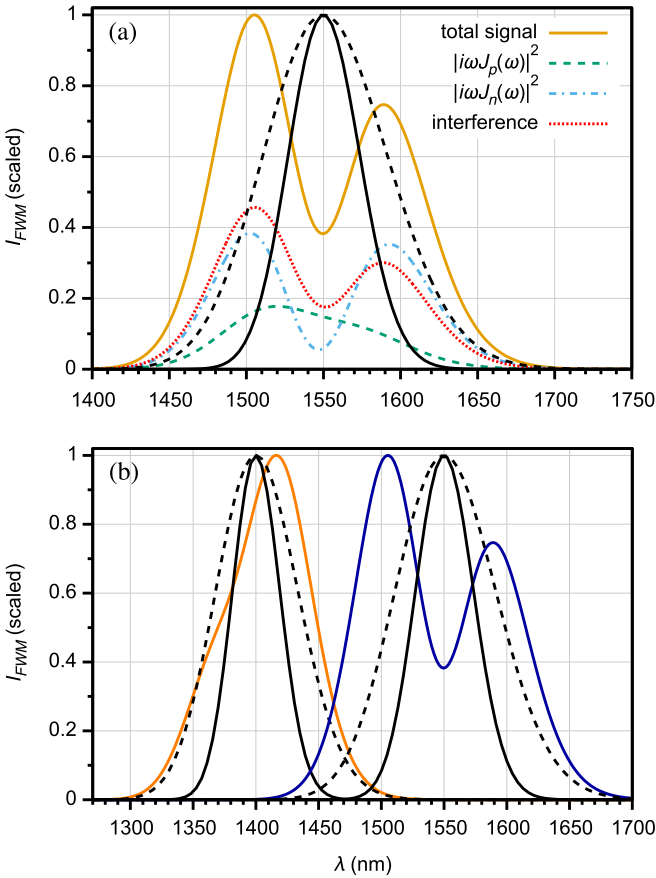
FIG. 3. FWM intensity in the frequency domain $|\omega \mathbf{J}_p(\omega) + \omega \mathbf{J}_n(\omega)|^2$. The black solid and dashed lines correspond to the squared Fourier transform of $E(t)$ and $[E(t)]^3$, i.e., $|E(\omega)|^2$ and $|E(\omega)|^6$, respectively. (a) The FWM signal for $\lambda_L = 1550$ nm along with individual contributions. The parameters are the same as in Fig. 2. (b) The right spectrum is the same as in (a); for the left one we changed only the excitation wavelength to $\lambda_L = 1400$ nm (both spectra are normalized). This roughly matches the excitation conditions used in the experiment (compare Fig. 4).

FIG. 4. Normalized transmission and FWM spectra of the CdTe and GaAs samples at a temperature of 10 K. The FWM spectra have been integrated over a time delay of 125 fs around the zero time delay between the two excitation pulses and are subtracted by the uniform stray light of the excitation pulses. While the directly transmitted pulses (dotted lines) represent the spectrum of the respective excitation pulses, the FWM signals (solid lines) show a distinct spectral broadening.

very small. Nevertheless, this explains why the interference term in Fig. 2(a) becomes positive again at about $t = 40$ fs.

The time-domain FWM signal with two peaks [see Fig. 2(a)] leads to the two peaks in the FWM spectrum; see Fig. 3(a), where the minimum in the center, i.e., near ω_L, is a direct consequence of the close to π phase shift in the time domain. Due to the reduction of certain spectral components, the FWM intensity spectrum $I_{FWM}(\omega)$ appears broader than the squared Fourier transform of $[E(t)]^3$.

Figure 3(b) shows two FWM spectra, with excitation conditions roughly matching those in the experiment shown in Fig. 4. For excitation with higher frequency ($\lambda_L = 1400$ nm), only a single peak appears instead of two; however, there still exists a weak separation into redshifted and blueshifted components. This is due to the only partial destructive interference, as mentioned above. In Fig. 3(b) we have chosen the same T_2 for each λ_L.

The agreement between the simulations and the experimental spectra could be further improved by assuming a shorter T_2 for the higher-frequency excitation (not shown);

however, since we model dephasing and relaxation phenomenologically, we focus here on demonstrating the principle effects and refrain from fitting and optimization in this initial study. In our model with an infinite T_1, the dephasing time T_2 has a significant influence on the total intensity and the spectral shape of the FWM signal. For a short T_2 the partial signal from $J_{n,n^{(2)}}$ is large and significantly delayed, resulting in a strong FWM at low frequencies. In the opposite case, the blueshifted components become more dominant, and the total signal is weaker.

III. EXPERIMENTAL RESULTS

To experimentally confirm these theoretical predictions we have performed spectrally resolved FWM experiments on a 900-μm-thick sample of bulk CdTe as well as a 500-μm-thick sample of bulk GaAs. The experiments are performed with a 1-kHz regenerative amplifier that emits 35-fs-long pulses at a central wavelength of 800 nm. This output drives an optical parametric amplifier that enables us to tune the excitation wavelength. For our experiments we choose central wavelengths of either 1400 or 1550 nm. Subsequently, the output of the optical parametric amplifier is divided into two pulses of equal intensity by means of a beam splitter. One of the two pulses passes a delay line before both pulses are focused onto the sample. The FWM signal, which is self-diffracted in the direction of $2\mathbf{k}_2 - \mathbf{k}_1$, is analyzed by means of a grating spectrometer. The spectrometer has a GaInAs detector line which allows us to detect photons from 900 to about 1600 nm.

First, we performed FWM experiments at the half-bandgap energy. For this we selected an excitation wavelength of 1550 nm (0.8 eV) and cooled the CdTe sample down to 10 K in a continuous-flow cryostat using liquid helium. At this
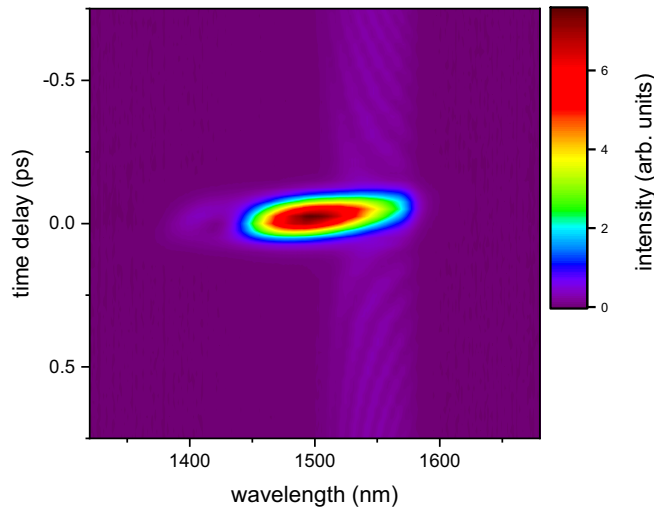
FIG. 5. Contour plot of the self-diffracted light in the direction of $2\mathbf{k}_2 - \mathbf{k}_1$ of a 500-μm-thick GaAs sample. The intensity of the detected light is reflected by the color scale. For a time delay of the two excitation pulses close to 0 ps a pronounced FWM signal is observed, while for larger time delays between both pulses only comparatively weak signals of stray light are detected. The FWM signal is substantially broadened compared to the stray light of the excitation pulses.

temperature, the band gap of CdTe is about 1.6 eV (775 nm) [79], so the excitation wavelength of 1550 nm corresponds precisely to half the band gap energy. The resulting FWM spectrum is shown in Fig. 4 together with the transmitted optical pulse for a pump fluence of 3.17 mJ/cm^2.

As theoretically predicted, we observe a clear spectral broadening of the FWM signal (blue line) compared to the directly transmitted optical pulse (black dashed line). While the intensity of the excitation pulse decreases rapidly towards zero for wavelengths below 1500 nm, the FWM signal is significantly broadened towards higher frequencies (shorter wavelengths). The maximum intensity of the FWM signal is blueshifted to 1520 nm, and there are two additional local interference maxima at 1430 and 1380 nm. In total, the FWM signal reaches down to almost 1350 nm and thus contains spectral components that are more than 100 nm below those of the optical excitation pulse. Above the central wavelength of 1550 nm a broadening of the FWM signal is also indicated in the experimental data. However, the strongly decreasing sensitivity of the detector above 1600 nm limits the significance of the data in this spectral range. To evaluate the spectral behavior of the FWM signal both above and below the excitation wavelength, the experiment is repeated at a central wavelength of 1400 nm. Here, a more or less symmetrical broadening of the FWM signal occurs (orange line in Fig. 4). In contrast to an excitation at 1550 nm, here a redshift of the FWM maximum in comparison to the optical excitation pulse is observed. A comparable redshift of the FWM peak has also been found for these excitation conditions in the theoretical modeling in Fig. 3(b).

These experimental observations are not limited to CdTe and cryogenic temperatures but also occur at bulk GaAs and room temperatures. Figure 5 shows a contour plot of the

spectral light intensity in the $2\mathbf{k}_2 - \mathbf{k}_1$ direction from a bulk GaAs sample. The sample is held at 10 K and excited at a central wavelength of 1550 nm with a pump fluence of 3.17 mJ/cm^2. For temporal overlap of the two excitation pulses, a distinct FWM signal is obtained which is spectrally broadened and blueshifted. Apart from the temporal overlap, only the nearly constant stray light of the excitation pulses is detected around 1550 nm. For better comparison with the CdTe sample, the FWM spectrum of the GaAs sample is plotted in Fig. 4 as well. Overall, we find a qualitatively similar response: the FWM signal of the GaAs sample shows a comparable spectral broadening and blueshift. Quantitatively, the FWM spectra of CdTe and GaAs differ particularly in the number and strength of the occurrence of the additional interference signatures. These interferences are much less pronounced for the GaAs sample. However, this behavior is consistent with the predictions of our numerical simulations. As described in Sec. II B, the development of interference patterns depends, among other things, on whether most interband transition frequencies $\omega_{\mathbf{k}}$ are greater or smaller than $2\omega_L$. Since the band gap of GaAs at 1.519 eV is smaller than that of CdTe, more $\omega_{\mathbf{k}}$ are smaller than $2\omega_L$, and therefore a less pronounced interference pattern is expected.

The fact that a qualitatively similar spectral broadening can be observed at different samples and sample temperatures suggests that this is a universal phenomenon of FWM signals for excitations close to half the band gap. On the other hand, quantitative differences such as the strength of the broadening or local interference maxima in the FWM spectra appear to be related to specific properties of the sample and their coherent dynamics.

IV. SUMMARY

We analyzed FWM performed with off-resonant pulses that have frequencies close to half the band gap frequency using microscopic models which include the dynamics of the electronic excitations. Although already for a simple two-level model some broadening of the FWM spectra originating simply from off-resonantly excited nonlinearities is obtained, a more realistic two-band model shows more complex signatures in both the time- and spectrally resolved FWM signals. These originate from several pathways which correspond to different combinations of inter- and intraband excitations that contribute to FWM. The significant broadening and structure of the FWM spectra that are obtained from numerical solutions of the SBEs are in good qualitative agreement with experimental results. Our findings offer several possibilities to analyze the dynamics of optical nonlinearities, electronic couplings, and many-body effects using strongly off-resonant excitations.
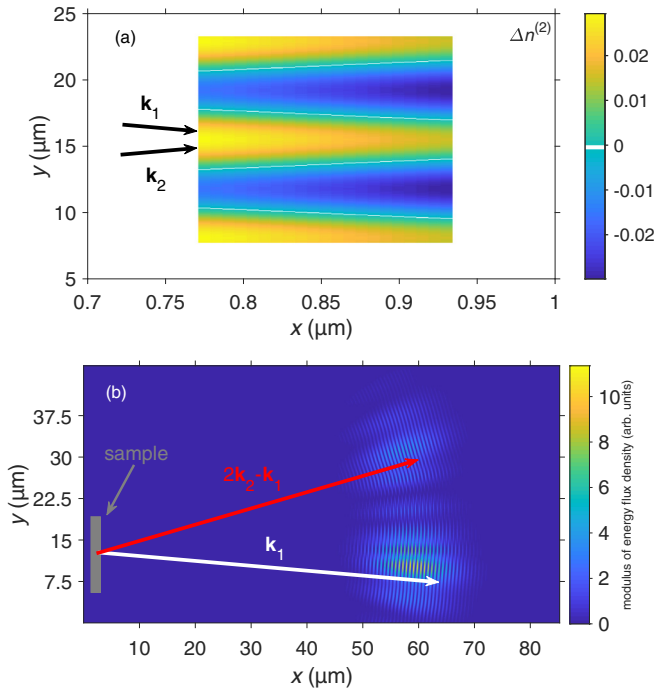
FIG. 6. (a) Snapshot of the transient density grating $\Delta n^{(2)}$ at $t = 10$ fs generated by the interference of two incident plane-wave pulses which propagate in the $\mathbf{k}_1$ and $\mathbf{k}_2$ directions, respectively. The sample medium is described as a small slab with a homogeneous density of two-level systems ($10^{24}/\mathrm{cm}^3$) with transition dipoles $|d| = 0.624$ eÅ. The transition energy of the two-level systems is $\hbar\omega_{cv} = 1.6$ eV; the incident pulses have a frequency of $\omega_L = 0.6\omega_{cv}$, have a Gaussian temporal envelope with $\bar{t} = 55$ fs, and have maxima of their envelopes at $x = 0.3875\,\mu$m for $t = 0$. (b) Snapshot of the energy flux density of the third-order electromagnetic field at 200 fs. At this time the diffracted pulses have traveled about 60 μm. The FWM direction of $2\mathbf{k}_2 - \mathbf{k}_1 = \mathbf{k}_2 + (\mathbf{k}_2 - \mathbf{k}_1)$ is indicated by the red arrow. In addition, a second pulse diffracted into the direction of the first pulse $\mathbf{k}_1 = \mathbf{k}_2 - (\mathbf{k}_2 - \mathbf{k}_1)$, which corresponds to a pump-probe signal, is visible. The indicated thickness of the sample (gray) is not to scale.

APPENDIX: NUMERICAL SOLUTIONS OF THE MAXWELL-BLOCH EQUATIONS FOR A TWO-DIMENSIONAL MODEL SYSTEM

Besides solving Eqs. (1) and (2), we also performed numerical model simulations of the Maxwell-Bloch equations in two spatial dimensions using the finite-difference time-domain (FDTD) method [80–82]. In these model calculations we consider a thin rectangular slab which contains a homogeneous spatial density of two-level systems and describes

two incident pulses with a finite spatial width arriving at the sample under an angle. These simulation results confirm the existence of a transient density grating $n^{(2)}$ at second order which is generated by the spatiotemporal interference of the two off-resonant excitation pulses. Furthermore, the numerical solutions of the Maxwell-Bloch equations which include, as the only nonlinearity, the Pauli blocking of the two-level systems as contained in Eqs. (1) and (2) demonstrate the emission of a finite FWM signal in the $2\mathbf{k}_2 - \mathbf{k}_1$ direction for off-resonant excitation [83]. Thus the density grating, i.e., the spatially varying occupation of the upper level of the two-level systems, acts similar to a Kerr nonlinearity.

The numerical solution of the Maxwell-Bloch equations is performed using a predictor-corrector algorithm which was first introduced by Ziolkowski *et al.* [81]. This approach is based on finite differencing of the coupled Maxwell's curl equations in space and time [80]. In our two-dimensional FDTD simulations we consider TM$_z$ modes as the source. The incident pulses are initialized at an angle of $\pm 5°$ using the total-field/scattered-field technique (TF/SF). [81] The sample, i.e., a thin slab containing a homogeneous density of two-level systems, is placed inside the TF region and extends from 775 to 930 nm in the x direction and from 7.75 to 23.25 μm in the y direction (see Fig. 6). In order to avoid artificial reflections at the outer surface of the FDTD simulation space we apply perfectly matched layer boundary conditions via auxiliary fields [82]. To keep the numerical requirements within reasonable limits, we considered a very small slab which, however, is still sufficient to highlight the essential physics, i.e., the generation of a transient density grating the emission of a FWM signal originating from the nonlinearity of the two-level systems.

We use a perturbative expansion in powers of the incident pulses to determine the emitted radiation caused by the third-order interband coherence $p^{(3)}$. This leads to three simulation spaces, two linear ones for each of the incident fields and one for the third-order excitation and fields, which are solved in the FDTD simulations [83]. The two linear interband coherences $p^{(1)}$ induced by each of the incident fields generate at second order a transient density grating $\Delta n^{(2)}$ [see Fig. 6(a)]. The interaction between the second pulse and the density grating leads to the nonlinear polarization $p^{(3)}$, whose second time derivative is the source of the field emitted in the FWM direction $2\mathbf{k}_2 - \mathbf{k}_1$. In Fig. 6(b) besides the emission into the FWM direction, also a field propagating into $\mathbf{k}_1$ corresponding to a pump-probe experiment is visible. The temporal dynamics and spectra of the FWM emission including propagation are very close to the results shown in Fig. 1.

[1] L. Schultheis, M. D. Sturge, and J. Hegarty, Appl. Phys. Lett. **47**, 995 (1985).

[2] L. Schultheis, J. Kuhl, A. Honold, and C. W. Tu, Phys. Rev. Lett. **57**, 1635 (1986).

[3] E. O. Göbel, K. Leo, T. C. Damen, J. Shah, S. Schmitt-Rink, W. Schäfer, J. F. Müller, and K. Köhler, Phys. Rev. Lett. **64**, 1801 (1990).

[4] M. Wegener, D. S. Chemla, S. Schmitt-Rink, and W. Schäfer, Phys. Rev. A **42**, 5675 (1990).

[5] M. Lindberg, R. Binder, and S. W. Koch, Phys. Rev. A **45**, 1865 (1992).

[6] M. Koch, J. Feldmann, G. von Plessen, E. O. Göbel, P. Thomas, and K. Köhler, Phys. Rev. Lett. **69**, 3631 (1992).

[7] K. Leo, J. Shah, T. C. Damen, A. Schulze, T. Meier, S. Schmitt-Rink, P. Thomas, E. O. Göbel, S. L. Chuang, M. S. C. Luo, W. Schäfer, K. Köhler, and P. Ganser, IEEE J. Quantum Electron. **28**, 2498 (1992).

[8] K.-H. Pantke, P. Schillak, B. S. Razbirin, V. G. Lyssenko, and J. M. Hvam, Phys. Rev. Lett. **70**, 327 (1993).

[9] R. Hellmann, M. Koch, J. Feldmann, S. T. Cundiff, E. O. Göbel, D. R. Yakovlev, A. Waag, and G. Landwehr, Phys. Rev. B **48**, 2847(R) (1993).

[10] A. Lohner, K. Rick, P. Leisching, A. Leitenstorfer, T. Elsaesser, T. Kuhn, F. Rossi, and W. Stolz, Phys. Rev. Lett. **71**, 77 (1993).

[11] D. S. Kim, J. Shah, T. C. Damen, L. N. Pfeiffer, and W. Schäfer, Phys. Rev. B **50**, 5775(R) (1994).

[12] F. Jahnke, M. Koch, T. Meier, J. Feldmann, W. Schäfer, P. Thomas, S. W. Koch, E. O. Göbel, and H. Nickel, Phys. Rev. B **50**, 8114 (1994).

[13] S. T. Cundiff, M. Koch, W. H. Knox, J. Shah, and W. Stolz, Phys. Rev. Lett. **77**, 1107 (1996).

[14] M. Koch, J. Shah, and T. Meier, Phys. Rev. B **57**, R2049(R) (1998).

[15] R. A. Kaindl, S. Lutgen, M. Woerner, T. Elsaesser, B. Nottelmann, V. M. Axt, T. Kuhn, A. Hase, and H. Künzel, Phys. Rev. Lett. **80**, 3575 (1998).

[16] P. Borri, W. Langbein, J. Mørk, J. M. Hvam, F. Heinrichsdorff, M.-H. Mao, and D. Bimberg, Phys. Rev. B **60**, 7784 (1999).

[17] M. Buck, L. Wischmeier, S. Schumacher, G. Czycholl, F. Jahnke, T. Voss, L. Rückmann, and J. Gutowski, Eur. Phys. J. B **42**, 175 (2004).

[18] M. Stein, C. Lammers, P.-H. Richter, C. Fuchs, W. Stolz, M. Koch, O. Vänskä, M. J. Weseloh, M. Kira, and S. W. Koch, Phys. Rev. B **97**, 125306 (2018).

[19] H. Haug and S. W. Koch, *Quantum Theory of the Optical and Electronic Properties of Semiconductors*, 5th ed. (World Scientific, Singapore, 2009).

[20] T. Meier, P. Thomas, and S. W. Koch, *Coherent Semiconductor Optics: From Basic Concepts to Nanostructure Applications* (Springer, Berlin, 2007).

[21] T. Yajima and Y. Taira, J. Phys. Soc. Jpn. **47**, 1620 (1979).

[22] S. Weiser, T. Meier, J. Möbius, A. Euteneuer, E. J. Mayer, W. Stolz, M. Hofmann, W. W. Rühle, P. Thomas, and S. W. Koch, Phys. Rev. B **61**, 13088 (2000).

[23] S. T. Cundiff, Opt. Express **16**, 4639 (2008).

[24] B. L. Wilmer, F. Passmann, M. Gehl, G. Khitrova, and A. D. Bristow, Phys. Rev. B **91**, 201304(R) (2015).

[25] M. Lindberg and S. W. Koch, Phys. Rev. B **38**, 3342 (1988).

[26] V. M. Axt and A. Stahl, Z. Phys. B **93**, 195 (1994); **93**, 205 (1994).

[27] M. Lindberg, Y. Z. Hu, R. Binder, and S. W. Koch, Phys. Rev. B **50**, 18060 (1994).

[28] B. F. Feuerbacher, J. Kuhl, and K. Ploog, Phys. Rev. B **43**, 2439 (1991).

[29] S. Bar-Ad and I. Bar-Joseph, Phys. Rev. Lett. **68**, 349 (1992).

[30] D. J. Lovering, R. T. Phillips, G. J. Denton, and G. W. Smith, Phys. Rev. Lett. **68**, 1880 (1992).

[31] K. Bott, O. Heller, D. Bennhardt, S. T. Cundiff, P. Thomas, E. J. Mayer, G. O. Smith, R. Eccleston, J. Kuhl, and K. Ploog, Phys. Rev. B **48**, 17418 (1993).

[32] J.-Y. Bigot, A. Daunois, J. Oberle, and J.-C. Merle, Phys. Rev. Lett. **71**, 1820 (1993).

[33] K.-H. Pantke, D. Oberhauser, V. G. Lyssenko, J. M. Hvam, and G. Weimann, Phys. Rev. B **47**, 2413 (1993).

[34] E. J. Mayer, G. O. Smith, V. Heuckeroth, J. Kuhl, K. Bott, A. Schulze, T. Meier, D. Bennhardt, S. W. Koch, P. Thomas, R. Hey, and K. Ploog, Phys. Rev. B **50**, 14730 (1994).

[35] E. J. Mayer, G. O. Smith, V. Heuckeroth, J. Kuhl, K. Bott, A. Schulze, T. Meier, S. W. Koch, P. Thomas, R. Hey, and K. Ploog, Phys. Rev. B **51**, 10909 (1995).

[36] T. F. Albrecht, K. Bott, T. Meier, A. Schulze, M. Koch, S. T. Cundiff, J. Feldmann, W. Stolz, P. Thomas, S. W. Koch, and E. O. Göbel, Phys. Rev. B **54**, 4436 (1996).

[37] W. Langbein, T. Meier, S. W. Koch, and J. M. Hvam, J. Opt. Soc. Am B **18**, 1318 (2001).

[38] H. Wang, K. B. Ferrio, D. G. Steel, Y. Z. Hu, R. Binder, and S. W. Koch, Phys. Rev. Lett. **71**, 1261 (1993).

[39] H. Wang, K. B. Ferrio, D. G. Steel, P. R. Berman, Y. Z. Hu, R. Binder, and S. W. Koch, Phys. Rev. A **49**, R1551(R) (1994).

[40] Y. Z. Hu, R. Binder, S. W. Koch, S. T. Cundiff, H. Wang, and D. G. Steel, Phys. Rev. B **49**, 14382 (1994).

[41] T. Rappen, U.-G. Peter, M. Wegener, and W. Schäfer, Phys. Rev. B **49**, 10774(R) (1994).

[42] T. Aoki, G. Mohs, M. Kuwata-Gonokami, and A. A. Yamaguchi, Phys. Rev. Lett. **82**, 3108 (1999).

[43] S. Mukamel, *Principles of Nonlinear Optical Spectroscopy* (Oxford University Press, Oxford, 1995).

[44] C. N. Borca, T. Zhang, X. Li, and S. T. Cundiff, Chem. Phys. Lett. **416**, 311 (2005).

[45] T. Zhang, I. Kuznetsova, T. Meier, X. Li, R. P. Mirin, P. Thomas, and S. T. Cundiff, Proc. Natl. Acad. Sci. USA **104**, 14227 (2007).

[46] D. B. Turner and K. A. Nelson, Nature (London) **466**, 1089 (2010).

[47] I. Gur-Arie and S. Bar-Ad, Phys. Rev. B **65**, 125311 (2002).

[48] J. Reif, R. P. Schmid, and T. Schneider, Appl. Phys. B **74**, 745 (2002).

[49] K. Dota, J. A. Dharmadhikari, D. Mathur, and A. K. Dharmadhikari, Appl. Phys. B **107**, 703 (2012).

[50] J. A. Dharmadhikari, K. Dota, D. Mathur, and A. K. Dharmadhikari, Appl. Phys. B **122**, 140 (2016).

[51] S. Ghimire, A. D. DiChiara, E. Sistrunk, P. Agostini, L. F. DiMauro, and D. A. Reis, Nat. Phys. **7**, 138 (2011).

[52] O. Schubert, M. Hohenleutner, F. Langer, B. Urbanek, C. Lange, U. Huttner, D. Golde, T. Meier, M. Kira, S. W. Koch, and R. Huber, Nat. Photonics **8**, 119 (2014).

[53] G. Vampa, T. J. Hammond, N. Thiré, B. E. Schmidt, F. Légaré, C. R. McDonald, T. Brabec, and P. B. Corkum, Nature (London) **522**, 462 (2015).

[54] M. Hohenleutner, F. Langer, O. Schubert, M. Knorr, U. Huttner, S. W. Koch, M. Kira, and R. Huber, Nature (London) **523**, 572 (2015).

[55] T. T. Luu, M. Garg, S. Yu. Kruchinin, A. Moulet, M. Th. Hassan, and E. Goulielmakis, Nature (London) **521**, 498 (2015).

[56] S. Yu. Kruchinin, F. Krausz, and V. S. Yakovlev, Rev. Mod. Phys. **90**, 021002 (2018).

[57] M. Wegener, *Extreme Nonlinear Optics* (Springer, Berlin, 2005).

[58] D. Golde, T. Meier, and S. W. Koch, Phys. Rev. B **77**, 075330 (2008).

[59] D. Golde, M. Kira, T. Meier, and S. W. Koch, Phys. Status Solidi B **248**, 863 (2011).

[60] G. Vampa, C. R. McDonald, G. Orlando, D. D. Klug, P. B. Corkum, and T. Brabec, Phys. Rev. Lett. **113**, 073901 (2014).

[61] T. Higuchi, M. I. Stockman, and P. Hommelhoff, Phys. Rev. Lett. **113**, 213901 (2014).

[62] A. A. Lanin, E. A. Stepanov, A. B. Fedotov, and A. M. Zheltikov, Optica **4**, 516 (2017).

[63] X. Song, R. Zuo, S. Yang, P. Li, T. Meier, and W. Yang, Opt. Express **27**, 2225 (2019).

[64] M. Sheik-Bahae, D. C. Hutchings, D. J. Hagan, and E. W. Van Stryland, IEEE J. Quantum Electron. **27**, 1296 (1991).

[65] A. A. Said, M. Sheik-Bahae, D. J. Hagan, T. H. Wei, J. Wang, J. Young, and E. W. Van Stryland, J. Opt. Soc. Am. B **9**, 405 (1992).

[66] J. A. Bolger, A. K. Kar, B. S. Wherrett, R. DeSalvo, D. C. Hutchings, and D. J. Hagan, Opt. Commun. **97**, 203 (1993).

[67] J. E. Sipe and E. Ghahramani, Phys. Rev. B **48**, 11705 (1993).

[68] C. Aversa, J. E. Sipe, M. Sheik-Bahae, and E. W. Van Stryland, Phys. Rev. B **50**, 18073 (1994).

[69] C. Aversa and J. E. Sipe, Phys. Rev. B **52**, 14636 (1995).

[70] W.-R. Hannes and T. Meier, Phys. Rev. B **99**, 125301 (2019).

[71] R. Atanasov, A. Haché, J. L. P. Hughes, H. M. van Driel, and J. E. Sipe, Phys. Rev. Lett. **76**, 1703 (1996).

[72] A. Haché, Y. Kostoulas, R. Atanasov, J. L. P. Hughes, J. E. Sipe, and H. M. van Driel, Phys. Rev. Lett. **78**, 306 (1997).

[73] R. D. R. Bhat and J. E. Sipe, Phys. Rev. Lett. **85**, 5432 (2000).

[74] M. J. Stevens, A. L. Smirl, R. D. R. Bhat, A. Najmaie, J. E. Sipe, and H. M. van Driel, Phys. Rev. Lett. **90**, 136603 (2003).

[75] J. Hübner, W. W. Rühle, M. Klude, D. Hommel, R. D. R. Bhat, J. E. Sipe, and H. M. van Driel, Phys. Rev. Lett. **90**, 216601 (2003).

[76] H. T. Duc, T. Meier, and S. W. Koch, Phys. Rev. Lett. **95**, 086606 (2005).

[77] L. Allen and J. H. Eberly, *Optical Resonance and Two-Level Atoms* (Wiley, New York, 1975).

[78] H. T. Duc, Q. T. Vu, T. Meier, H. Haug, and S. W. Koch, Phys. Rev. B **74**, 165328 (2006).

[79] G. Fonthal, L. Tirado-Mejía, J. I. Marín-Hurtado, H. Ariza-Calderón, and J. G. Mendoza-Alvarez, J. Phys. Chem. Solids **61**, 579 (2000).

[80] A. Taflove and S. C. Hagness, *Computational Electrodynamics: The Finite-Difference Time-Domain Method*, 3rd ed. (Artech House, Norwood, MA, 2005).

[81] R. W. Ziolkowski, J. M. Arnold, and D. M. Gogny, Phys. Rev. A **52**, 3082 (1995).

[82] U. S. Inan and R. A. Marshall, *Numerical Electromagnetics: The FDTD Method* (Cambridge University Press, New York, 2011).

[83] A. Trautmann, M.Sc. thesis, Universität Paderborn, 2018.